Pure Appl. Chem., Vol. 81, No. 10, pp. 1889–1901, 2009.
doi:10.1351/PAC-CON-08-07-06

Trace gas adsorption thermodynamics at the air–water interface: Implications in atmospheric chemistry*

Kalliat T. Valsaraj

Cain Department of Chemical Engineering, Louisiana State University, Baton Rouge, LA 70803, USA

Abstract: The thermodynamics of adsorption of gaseous organic compounds such as polycyclic aromatic hydrocarbons (PAHs) on water films is reviewed and discussed. The various experimental methods available to determine the thermodynamic equilibrium constant and the structure–activity relationships to correlate and estimate the same are reviewed. The atmospheric implications of the adsorption and oxidation of PAHs at the air–water interface of thin films of water such as existing in fog droplets, ice films, and aerosols are also enumerated.

Keywords: atmospheric oxidation; gas adsorption; polycyclic aromatic hydrocarbons; thermodynamics; water thin films.

INTRODUCTION

The air–water interface is the largest interface in the environment [1]. It exists as bulk phases in contact (e.g., air–sea), one phase dispersed in the other (e.g., rain, fog, mist) or as a surface film in contact with a bulk phase (e.g., water films on aerosols, snow, and ice). Very thin water films that exist on aerosol particles, fog droplets, snow, and ice surfaces are likely to behave differently from a bulk water phase.

The distribution of a pollutant, i between the two bulk phases, is given by the equilibrium thermodynamic partition constant (Henry's constant) [2]

$$K_{wa} = \frac{C_i(\mathrm{aq})}{C_i(\mathrm{g})} \tag{1}$$

where C_i(aq) and C_i(g) are, respectively, the molar concentrations (mol m^{-3}) of the species i in the water (aq) and air (g) phases. When the partitioning involves the air–water interface (σ) and air (g), the equilibrium partition constant is given by [2]

$$K_{\sigma a} = \frac{\Gamma_i^{\sigma}}{C_i(\mathrm{g})} \tag{2}$$

where Γ_i^{σ} represents the surface concentration at the air–water interface (mol m^{-2}), and $K_{\sigma a}$ has units of m. Although a lot is known about the bulk phase relationship, much less information exists on the

*Paper based on a presentation at the 20th International Conference on Chemical Thermodynamics (ICCT 20), 3–8 August 2008, Warsaw, Poland. Other presentations are published in this issue, pp. 1719–1959.

interface partition constant, especially for environmentally significant compounds such as hydrophobic semivolatile organic compounds (SVOCs) and volatile organic compounds (VOCs). This paper is a review of the thermodynamics, methods of estimation, and existing data on the interface partition constants. We further review the data on the importance of surface adsorption and atmospheric oxidations of several compounds.

THERMODYNAMICS OF ADSORPTION AT THE AIR–WATER INTERFACE

We begin with the criteria of equal chemical potentials for a compound i in the bulk air and the air–water interface [2]

$$\mu_i^{0a} + RT\ \ell n\left(P_i \Big/ P^0\right) = \mu_i^{0\sigma} + RT\ \ell n\left(\gamma_i^{\sigma}\pi_i \Big/ \pi^0\right) \tag{3}$$

where P^0 = 101.325 kPa is the standard pressure for the gas phase, and π^0 = 0.06084 mN m^{-1} is the corresponding state standard surface pressure proposed by Kemball and Rideal [4], and γ_i^{σ} is included to consider nonideality in the surface phase. The Kemball–Rideal standard state is the two-dimensional equivalent of an ideal gas standard state [4]. The surface activity coefficient is an unknown function of the surface coverage or surface pressure, π_i. However, as defined $\gamma_i^{\sigma} \rightarrow 1$ as $\pi_i \rightarrow 0$. Therefore, the standard Gibbs free energy for the transfer of 1 mole from bulk air phase to the air–water interface is given by

$$\Delta_{\text{ads}}G^0 = -RT\ \ell n\left(\frac{\pi_i}{P_i}\cdot\frac{1}{\delta_0}\right) \tag{4}$$

where δ_0 is the ratio of the standard states or otherwise called the standard surface thickness (=6 × 10^{-10} m). Surface pressure π_i is a function of the partial pressure P_i, and, therefore, the ratio π_i/P_i represents the adsorption isotherm at the interface. Since the equation of state for the two-dimensional gaseous state is similar to that of the ideal gaseous state for the bulk air phase, π_i/P_i is the ratio Γ_i^{σ}/C_i(g). This is given by a Langmuir adsorption isotherm of the following form [41]:

$$\frac{\Gamma_i^{\sigma}}{C_i(\text{g})} = \frac{\Gamma_i^{\sigma,\max}}{C_{i,1/2} + C_i(\text{g})} \tag{5}$$

where $\Gamma_i^{\sigma,\max}$ is the maximum monolayer adsorption capacity of i (mol m^{-2}) and represents the gas phase concentration of i (mol m^{-3}) at half monolayer saturation. For most gaseous VOCs and SVOCs of environmental interest, $C_{i,1/2} >> C_i$(g), and hence a linear adsorption isotherm (as given in eq. 2 where $K_{\sigma a} = \Gamma_i^{\sigma,\max}/C_{i,1/2}$) will suffice. Thus

$$\Delta_{\text{ads}}G^0 = -RT\ \ell n\left(\frac{K_{\sigma a}}{\delta_0}\right) \tag{6}$$

Thus, experimental estimates of $K_{\sigma a}$ give us the free energy for adsorption. Further, utilizing the Gibbs–Helmholtz relationship, we can obtain the enthalpy of adsorption from the temperature dependence of $K_{\sigma a}$.

$$\frac{d}{dT}\left[\ell n\left(K_{\sigma a} \Big/ \delta_0\right)\right] = \frac{\Delta_{\text{ads}}H^0}{RT^2} \tag{7}$$

Further, the entropy of adsorption is obtained from

$$\Delta_{\text{ads}}S^0 = \frac{\left(\Delta_{\text{ads}}H^0 - \Delta_{\text{ads}}G^0\right)}{T} \tag{8}$$

In addition to the Kemball–Rideal standard state described above, other authors have used different standard state definitions such as: (i) a unit surface concentration (1 mol m^{-2}) standard state, (ii) a unit surface pressure (1 mN m^{-1}) standard state, and (iii) a unit surface mole fraction ($x_i^{\sigma} = 1$) standard state. Note that the choice of standard state will influence the numerical value of the surface free energy and entropy. It will also affect the surface activity coefficients since the degree of surface non-ideality is relative to the chosen standard state. However, the molar enthalpy of adsorption is less sensitive to the choice of standard state.

The free energy for the transfer of 1 mol of solute from air to bulk water is given by

$$\Delta_{a\to w}G^0 = -RT\ \ell n\, K_{wa} \tag{9}$$

where the aqueous phase standard state is the ideal solution at unit molar concentration, 1 mol m^{-3}.

EXPERIMENTAL DATA ON AIR–WATER INTERFACE PARTITION CONSTANT

Several experimental measurements of the air–water interface partition constant have been reported in the literature for environmentally relevant VOCs and SVOCs. In general, such measurements are difficult for water surfaces due to the volatility of water, small extent of adsorption of gases, and the difficulties involved in the preparation of clean water surfaces. Moreover, in most cases, the relatively low vapor pressures of VOCs and SVOCs and the low adsorbed concentrations make it difficult to obtain reproducible results. Extrapolation from high concentrations to the environmentally relevant low concentrations is fraught with uncertainties.

Conventional surface pressure measurements

Ottewill and coworkers [5–7] studied the adsorption of low-molecular-weight, volatile, aromatic hydrocarbon vapors at the air–water interface in the early 1950s. They used the conventional surface pressure (tension) measurements using a dipping plate technique and provided adsorption isotherms for various hydrocarbons (benzene, toluene, *o*-xylene, chlorobenzene) and alcohols and showed that there is finite enrichment at the interface for these compounds. Others [8–10] expanded the work to include low-molecular-weight, aliphatic hydrocarbons (C_5–C_{16} alkanes). More recently, surface pressures of an aromatic molecule (benzene) were obtained using an axi-symmetric pendant drop shape analysis procedure [11]. Donaldson and coworkers [12,13] used capillary rise method to obtain the adsorption isotherms for several atmospherically relevant gases (NH_3, methylamines, C_1–C_4 alcohols, and acids) at the air–water interface.

The above methods are only reliable for those gases that have substantial partial pressures so that measurable adsorption can be obtained directly from surface pressure measurements using conventional techniques. They do not work for many atmospherically relevant SVOCs that have very low vapor pressure.

Indirect surface concentration measurements

There are several indirect methods for obtaining surface concentrations, two of which have been most recently explored. The first one involves inverse gas chromatography (IGC), and the second one involves uptake measurements in a thin film flow reactor.

IGC involves the use of a known film thickness of water coated in a chromatographic column that retains a gaseous organic compound via both bulk dissolution and adsorption on the water surface. The net retention volume (m^3) of an organic solute per kilogram of the solid adsorbent is then composed of two parts

$$V_N = K_{\sigma a} A_w + K_{wa} V_w \tag{10}$$

where A_w and V_w are, respectively, the air–water interfacial area ($m^2\ kg^{-1}$) and water volume ($m^3\ kg^{-1}$) on the column. Experimentally, the net retention volume is obtained from $K_C V_M$, where K_C is the capacity factor and V_M is the volume of gas-phase per kg of adsorbent. The capacity factor is obtained from $K_C = (t_R/t_M) - 1$, where t_R and t_M are, respectively, the retention time of the solute and that of a non-adsorbing solute (methane). By plotting the value of V_N/V_W vs. A_W/V_W, we can obtain the values of $K_{\sigma a}$ (as slope) and K_{wa} (from the intercept). The experiments can be repeated to obtain the temperature dependence of the partition constants.

Karger and coworkers [3] obtained the gas–water partition constants for low-molecular-weight organic solutes (C_5–C_8 alkanes, cycloalkanes, chloroalkanes, aromatic hydrocarbons, and esters) using this method. Dorris and Gray [14] used the method to obtain the adsorption of several *n*-alkanes at 298 K. Hoff et al. [15] used the procedure to obtain the partition constants for 35 atmospherically relevant organic molecules at 298 K and provided correlations for the same. Raja et al. [16] used IGC to obtain the partition constants for three specific polycyclic aromatic hydrocarbons (PAHs) (benzene, naphthalene, phenanthrene), which are atmospherically important and obtained the temperature dependence of the partition constants. More recently, Roth et al. [17] provided a comprehensive set of data at 298 K for 61 specific organic molecules using the IGC method.

In another series of work, our group showed that one could use a thin film of water in a cylindrical flow reactor to obtain the interface partition constant from uptake measurements [18]. In this method, a thin film of water is coated on a glass plate and placed inside a cylindrical reactor and exposed to a stream of a PAH vapor. The compound is detected at the outlet of the reactor using a GC/MS. The total equilibrium uptake ratio is given by the following [18,23]:

$$K_{wa}^{*} = K_{wa} + \frac{K_{\sigma a}}{\delta} \tag{11}$$

where δ is the water film thickness (m). The measured value of the overall partition constant (K_{wa}^{*}) is plotted against the inverse of the film thickness ($1/\delta$) to obtain the slope $K_{\sigma a}$. Naphthalene was used as the probe molecule in this case. The value obtained was $(2.7 \pm 0.1) \times 10^{-5}$ m and is compared with various other methods of estimations in Table 1.

Table 1 Thermodynamic parameters ($K_{\sigma a}$, $\Delta_{ads}G^0$, and $\Delta_{ads}H^0$) from experiments and molecular dynamics simulations for selected aromatic hydrocarbons.

	$K_{\sigma a}$/m	$\Delta_{ads}G^0$/kJ mol^{-1}		$\Delta_{ads}H^0$/kJ mol^{-1}	
Compound	Experimental	Experimental	Theory	Experimental	Theory
Benzene	$(4.3 \pm 0.1) \times 10^{-7}$ [16]	–16.3 ± 0.04 [16]	–15 [23]	–41 ± 2 [16]	–31 [39]
	4.9×10^{-7} [15]		–17 [25]	–41 [11]	–32 [40]
	4.1×10^{-7} [11]			–31 [6]	
	4.4×10^{-7} [15]				
Naphthalene	$(2.7 \pm 0.1) \times 10^{-5}$ [16]	–26.5 ± 0.1 [16]	–24 [23]	–67 ± 17 [16]	
Phenanthrene	3.3×10^{-2} [26]	–46 [16]	–35 [23]	–104 ± 36 [16]	

Correlations for air–water interface partition constants

There are two linear free energy relationships (LFERs) prescribed in the literature for $K_{\sigma a}$ based on the comprehensive data sets given above. These correlations are useful to obtain the partition constants for compounds that do not have reported values in the literature. The first correlation developed by Goss [19] used only 28 compounds and related $K_{\sigma a}$ to the subcooled liquid vapor pressures (P_i^*) of compounds at 288 K

$$\ell og\left(K_{\sigma a}/_{cm}\right) = -0.615\,\ell n\,P_i^* + 7.66\beta - 10.41 - \left[385\,\ell n\,P_i^* - 6037\beta - 6611\right]\left(\frac{1}{T} - \frac{1}{323}\right) \tag{12}$$

Later, Roth et al. [17] used a more comprehensive set of 61 molecules to obtain a better correlation at 288 K with the solute's hexadecane–air partition constants, K_{ha}

$$\ell og\left(K_{\sigma a}/_{m}\right) = 0.635\ell og\,K_{ha} + 3.60\alpha + 5.11\beta - 8.47 \tag{13}$$

where α and β are, respectively, the solute electron acceptor (H-bonding acidity) and electron donor (H-bonding basicity) of the molecule as defined by Abraham [20,21] and available in the literature.

Kelly et al. [22] provided a detailed analysis of the LFER for air–water interface partition constants using a basis set of 85 molecules and showed that very good predictions of the free energy of solvation at the air–water interface are possible using the atomic surface tensions developed from solvent descriptors. Thus, at present, correlations of the thermodynamic partition constants at the air–water interface are available.

Molecular dynamics simulations of adsorption at the air–water interface

It has been shown that molecular dynamics simulations can accurately predict the interfacial adsorption of aromatic molecules [23,24]. This lends support to the assertion that as a molecule travels from the air to the water, a pronounced free energy minimum is observed at the interface. This is directly reflected in the large surface excess observed for the molecule. For example, in Fig. 1 we show the theoretically obtained free energy profile for a molecule such as naphthalene. The free energy difference for adsorption from the gas phase is –24 kJ mol^{-1} with a hydration free energy of –10 kJ mol^{-1}. In other words, there is a significant free energy barrier to desorption of naphthalene from the air–water interface to the bulk water phase, whereas the adsorption at the interface from the gas phase is quite favorable. Similar simulations for benzene, phenanthrene, and anthracene also showed deep surface energy minima [24,25]. The free energy of adsorption varied in proportion to the molecular surface area. The free energy values were in good agreement with those reported for the PAHs from experiments (Table 1).

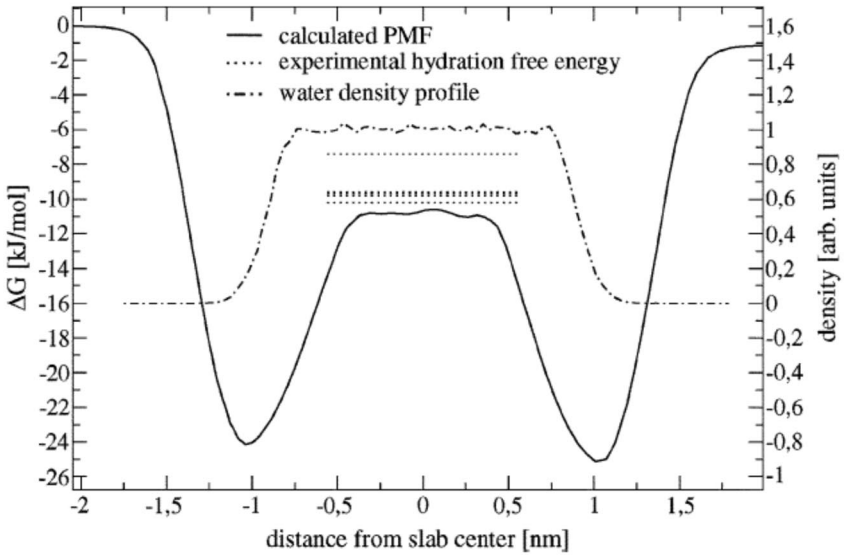

Fig. 1 Potential of mean force for moving a naphthalene molecule through the air–water interface of an aqueous slab (solid line) defined by the water density profile (broken line). Adapted from [23]. Note the deep minimum observed at the interface. The dashed lines represent the free energy of dissolution in bulk water obtained from experimental values of Henry's law constant for naphthalene between bulk air and water.

Direct spectroscopic studies of adsorption at the air–water Interface

Water surfaces are traditionally not amenable to typical high-vacuum surface science techniques such as particle scattering or scanning probe methods due to the high vapor pressure and mobility of the molecules at the surface. However, with the advent of modern nonlinear optical techniques, there is increasing use of spectroscopic studies toward understanding the water surfaces. These are useful to study mainly small polar and nonpolar molecules at the water surface. The various techniques currently employed to study water surfaces are: UV-photoelectron spectroscopy (PES) [43], X-ray photoelectron spectroscopy (XPS) [49], vibrational sum-frequency generation (VSFG) [44], second harmonic generation (SHG) [45], and reflection-absorption infrared spectroscopy (RAIRS) [46]. As long as the adsorbed molecules lie on or above the surface of water, the results obtained for water at lower temperatures such as amorphous solid water (ASW) surfaces and liquid water surfaces can be semi-quantitatively compared to one another [47,48].

ATMOSPHERIC IMPLICATIONS OF AIR–WATER INTERFACE PARTITIONING

The fact that most VOCs and SVOCs have a propensity for the air–water interface makes it inevitable that transport and reactions on droplets (fog, mist, dew, and rain) in the atmosphere, water films on aerosols and ice surfaces will be effected. These effects have been substantiated by experiments in the laboratory.

Experiments in laboratory scale falling droplet reactors have shown that there is a strong dependence of vapor uptake on droplet sizes. The net concentration of a VOC or SVOC on a droplet in contact with the compound is given by

$$C_i(\mathrm{aq}) = C_i^0(\mathrm{aq}) + \left(\frac{6}{d_P} \cdot \Gamma_i^\sigma\right) \tag{14}$$

where C_i^0 (aq) is the concentration (mol m^{-3}) in the bulk water phase (dispersed phase) and the term within the brackets denotes the surface concentration per unit volume of the droplet. The net concentration on the dispersed phase increases as the droplet diameter decreases. As diameter decreases, the net surface adsorbed concentration makes a larger contribution and the thermodynamic uptake coefficient shows the same size dependence

$$K_{wa}^{*} = K_{wa} + \left(\frac{6}{d_P}\right) K_{\sigma a} \tag{15}$$

Several field observations of uptake by fog droplets have shown that smaller droplets carry higher concentrations of pollutants in a foggy atmosphere [28], thus supporting the thermodynamic arguments given above. Field data on uptake into fog and dew droplets have indicated that there is substantial enrichment of pesticides, PAHs, esters, alkanes, and chlorinated alkanes from the interstitial air (Table 2). This enrichment is partly a result of colloidal organic matter in fog water that increases the aqueous phase solubility of gases. However, it is the increased specific surface area on small droplets that has been proposed as a likely reason for the enhanced partitioning [31]. Precipitation scavenging by dew and rain has also shown substantially higher concentrations in water than that predicted by bulk phase Henry's law equilibrium relationships [60,61]

Table 2 Enrichment of pesticides in fog and dew observed in field experiments [28,61].

Type of precipitation	Compound	Ranges of enrichment ratio, ε_H
Fog	Chlorpyrifos	7–260
	Parathion	4–310
	Diazinon	6–500
	Alachlor	4–13
	Malathion	1–6
	Methidathion	1–4
Dew	Dichloromethane	7
	Carbon tetrachloride	38
	1,2-Dichloroethane	9
	1,1,1-Trichloroethane	49
	Trichloroethylene	63
	Tetrachloroethylene	10.1
	Benzene	8
	Toluene	8
	o-Xylene	20
	m,*p*-Xylene12	

Note: Enrichment is defined as the ratio of observed fog-air partition constant to the thermodynamic equilibrium pure water–air Henry's constant $\left(\varepsilon_H = \frac{K_{wa}^{*}}{K_{wa}}\right)$.

In the laboratory it has been demonstrated that gases that adsorb to the air–water interface display high reactivity toward gaseous oxidants in the atmosphere. Molecular dynamics simulations and ab initio calculations have shown that several gaseous oxidants (ozone, singlet oxygen, hydroxyl radicals) also have high propensity for the air–water interface [35,38]. Donaldson et al. [29] were the first to provide direct evidence of atmospheric reactions of ozone with PAHs adsorbed at the air–water interface. Recent molecular dynamics simulations from our group have further provided proof for the simultaneous facile adsorption of ozone and PAH at the interface and the consequent high reaction probability

[47]. In the past, others have demonstrated that ozonation reaction at the interface for a phospholipid is enhanced [6]. Recently, Enami et al. [27] also showed that gas-phase ozone reacts with uric acid on the air–water interface at rates much higher than in the bulk phase. Our laboratory has shown that the ozonation reaction of PAHs on small aqueous droplets is considerably larger than the bulk phase reactions due to the heterogeneous bimolecular reaction of adsorbed ozone with PAH at the air–water interface [32].

The reaction at the surface is best described via a Langmuir–Hinshelwood mechanism, wherein two molecules (I = solute and Ox = Oxidant) are simultaneously adsorbed at the air–water interface and undergo a bimolecular reaction. In order to explain the overall dependence of the reaction rate constant on the oxidant and solute concentrations, the proposed rate (r_i^s/mol m^{-2} s^{-1}) is given by [29,42]

$$r_i^S = k_{2,\sigma}\Gamma_{Ox}^{\sigma}\Gamma_i^{\sigma} \tag{16}$$

In the above equation, $k_{2,\sigma}$/m^2 mol^{-1} s^{-1} represents the second-order Langmuir–Hinshelwood surface reaction rate constant. A Langmuir isotherm was assumed to represent the Ox adsorption, which gives the following equation [47]:

$$r_i^s = k_{2,\sigma}\cdot\left(\frac{\Gamma_{Ox}^{\max}C_{Ox}(\mathrm{g})}{C_{Ox,1/2}+C_{Ox}(\mathrm{g})}\right)\cdot\Gamma_i^{\sigma} = k_s\Gamma_i^{\sigma} \tag{17}$$

where k_s/s^{-1} is the overall rate constant for the surface reaction. As can be seen from the above equation, k_s is linear in C_{Ox}(g) for low values of C_{Ox}(g) and approaches an asymptotic value at high values of C_{Ox}(g). Such behavior has been noted for a number of cases where reactions at the air–water interface were fit to the following form:

$$k_S = \frac{k_{\max}C_{Ox}(\mathrm{g})}{C_{Ox,1/2}+C_{Ox}(\mathrm{g})} \tag{18}$$

The values of $k_{\max} = k_{2,\sigma}\Gamma_{Ox}^{\max}$ and $C_{Ox,1/2}$ obtained for the reaction of a typical PAH with ozone (oxidant) at the air–water interface are given in Table 3.

Table 3 Rate constants for uptake and reaction of SVOCs and gaseous oxidants at the air–water interface in different forms [18,26,29,30].

Nature of surface	SVOC	Ox	k_S/s^{-1}	$k_{\max}$/s^{-1}	$C_{Ox,1/2}$/ mol m^{-3}
Water surface	Anthracene	O_3		2.5×10^{-3}	2.1×10^{20}
Water (bulk)	Naphthalene	$O_2(^1\Delta_g)$	$(2.4 \pm 0.1) \times 10^{-5}$		
	Anthracence		$(1.7 \pm 0.3) \times 10^{-4}$		
Water–ice (surface)	Naphthalene	$O_2(^1\Delta_g)$	$(2.2 \pm 0.5) \times 10^{-4}$		
	Anthracence		$(1.06 \pm 0.05) \times 10^{-3}$		
Water (22 μm film)	Naphthalene	$O_2(^1\Delta_g)$	2.9×10^{-4}		
	Phenanthrene		6×10^{-5}		
Water (0.0125 m)	Naphthalene	$O_2(^1\Delta_g)$	2×10^{-6}		
	Phenanthrene		1×10^{-5}		

The oxidation of PAHs at the air–water interface by reaction with singlet oxygen [$O_2(^1\Delta_g)$] is also enhanced via adsorption. Several recent papers from our laboratory have investigated this phenomenon [18,26]. We have used thin films of water (22 to 800 μm) in a cylindrical flow reactor where adsorption

equilibrium was first attained by exposing the water films to PAH vapor. Subsequently, the surface adsorbed PAHs were exposed to UV light and reaction with singlet oxygen examined. The net photochemical reaction rate in a water film of thickness δ is composed of two processes: (i) a homogeneous reaction in the bulk fluid (water), and (ii) a heterogeneous reaction at the surface of the film. Thus, the overall rate constant is given by [16]

$$k_{\text{tot}} = k_w + k_S \cdot \frac{K_{\sigma a}}{K_{wa}} \cdot \frac{1}{\delta} \tag{19}$$

The above equation denotes that as $\delta \to 0$ (thin film), or $1/\delta \to \infty$, the rate constant is driven by the heterogeneous rate, whereas with $\delta \to \infty$ (bulk aqueous phase), the reaction is entirely homogeneous. The variation in k_{tot} for products formed by $O_2(^1\Delta_g)$ photooxidation of gaseous naphthalene and phenanthrene adsorbed at the air–water interface of films is shown in Fig. 2.

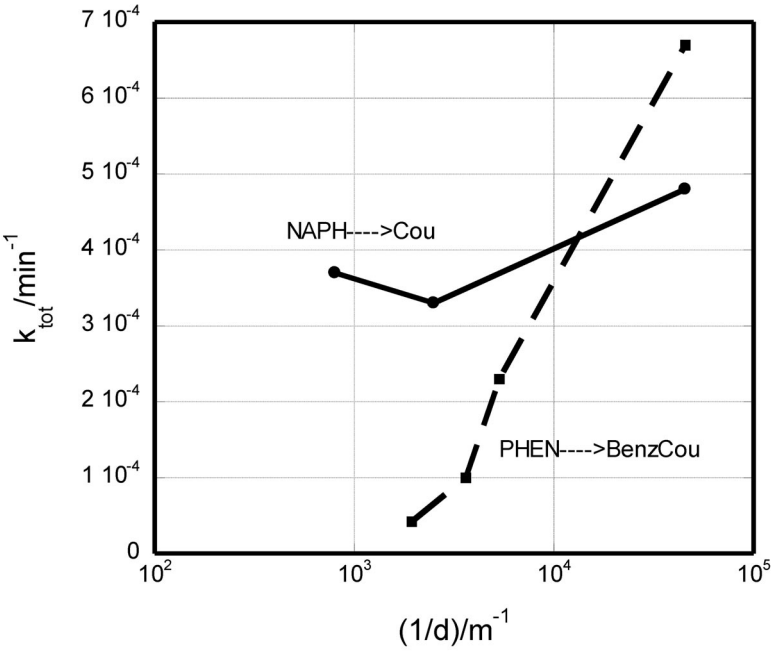

Fig. 2 The first-order rate constants for the formation of coumarin (Cou) and benzocoumarin (BenzCou) from the singlet oxygen photo-oxidation of adsorbed naphthalene (NAPH) and phenanthrene (PHEN), respectively, on water films of varying thickness [18,26]. Note that as δ decreases, there is a substantial increase in the rate constant.

Data from our work as well as those of others [18,26,30,37] show that the surface reaction rate increases considerably as one goes from the bulk solution to the thin water film and to the water–ice film (Table 3). The following hypothesis is offered (see Fig. 3): In the bulk aqueous phase, the reaction between PAH and *Ox* species is limited by the solvent-cage effect and small bulk liquid diffusion constant for the species. On the surface of thin water films, incomplete solvent-cage effect at the surface, enhanced surface concentration, and large surface diffusion constants of PAH and *Ox* species will lead to large surface reaction rates [33,34]. There is evidence that on the disordered water layer (quasi-liquid layer) on ice surfaces, PAH molecules will resist solvation and self-associate. Photon absorption by PAHs on ice surfaces appears to be greater than on water films, thus increasing the photolysis reaction on ice surfaces [37]. Further surface probe experiments are needed to corroborate the above hypotheses.

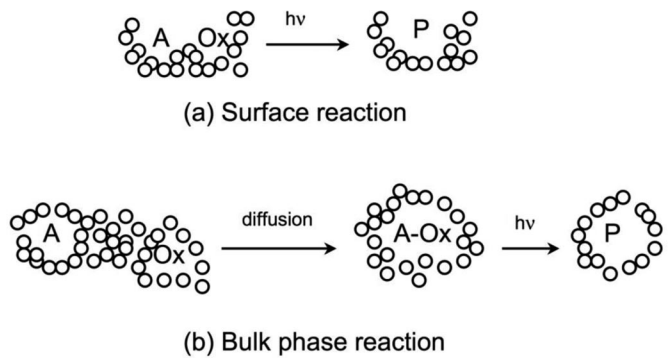

Fig. 3 Schematic of the increased surface reaction rate due to the decreased solvent-cage effect and enhanced surface concentration compared to diffusion-control and solvent cage effect in the bulk phase.

Consider a typical PAH (e.g., naphthalene) vapor. Its fate and transport at atmospheric aqueous surfaces (fog, rain, snow) are determined by thermodynamic equilibrium uptake at the interface and subsequent reaction (oxidation) at the surface. Typically, we consider reactive oxygen species, *Ox* [O_3, $OH^{\bullet}$, $O_2(^1\Delta_g)$] that can convert PAH to oxy-PAHs. Several homogeneous gas-phase oxidation processes compete with corresponding heterogeneous oxidation reactions on thin water films that occur on aerosols, fog droplets, and ice surfaces. In this section, we compare the characteristic time constants (τ) for the above processes in the atmosphere.

$$\text{Air phase:}\quad \tau_{\text{gas}} = \frac{1}{k_{2,a} C_{Ox}(g)}$$

$$\text{Film (water) phase:}\quad \tau_{\text{film}} = \frac{1}{\left(k_w + \frac{k_S}{\delta} \cdot \frac{K_{\sigma a}}{K_{wa}}\right) \cdot K_{wa}} \tag{20}$$

where $k_{2,a}$ is the homogeneous gas-phase second-order rate coefficient (m^3 $molecule^{-1}$ s^{-1}) with $C_{Ox}(g)$, the *Ox* concentration in the air phase, k_w is the pseudo-first order homogeneous rate coefficient (s^{-1}) in the liquid (water) phase, and k_S is the pseudo-first-order heterogeneous rate coefficient (s^{-1}) on the surface. k_w is given by $k_{2,w}C_{Ox}(aq)$, where $k_{2,w}$ is the second-order homogeneous rate coefficient (m^3 $molecule^{-1}$ s^{-1}) with $C_{Ox}(aq)$, the *Ox* concentration in the water phase. The values of the time constants obtained using parameters taken from the literature are given in Table 4. Clearly, heterogeneous oxidation in thin films by hydroxyl radical and singlet oxygen out-competes other oxidation pathways. Ozone oxidation is too slow and does not appear to be of significance in either gas-phase or thin-film oxidation. Similarly, gas-phase oxidation by hydroxyl radical also is slower than the thin film heterogeneous pathway. The significance of the uptake equilibrium at the air–water interface and subsequent oxidation is apparent from these calculations.

Table 4 Comparison of characteristic time constants for gas-phase homogeneous oxidation and thin water film (15 μm) heterogeneous oxidation for a typical PAH molecule (naphthalene).

Gas-phase oxidant	τ_{gas} (homogeneous)	τ_{film} (heterogeneous)
$^{\bullet}OH$	9 h	15 min
O_3	48 d	8 h
$^1O_2$	N/A	22 min

Parameters used in the calculations of time constants:
Bulk gas phase OH: $k_{2,a} = 2.4 \times 10^{-17}$ m^3 molecule^{-1} s^{-1}; $C_{OH}(g) = 1.4 \times 10^{12}$ molecule m^{-3} air.
Bulk gas phase O_3: $k_{2,a} = 2.0 \times 10^{-25}$ m^3 molecule^{-1} s^{-1}; $C_{O3}(g) = 1.2 \times 10^{18}$ molecule m^{-3} air.
Bulk liquid phase OH: $k_{2,w} = 1.2 \times 10^{-17}$ m^3 molecule^{-1} s^{-1}; $C_{OH}(aq) = 1.7 \times 10^{12}$ molecule m^{-3} liquid.
Bulk liquid phase O_3: $k_{2,w} = 12 \times 10^{-25}$ m^3 molecule^{-1} s^{-1}; $C_{O3}(aq) = 3.7 \times 10^{17}$ molecule m^{-3} liquid.
Water film: $^{\bullet}OH$: $k_w = 2.0 \times 10^{-5}$ s^{-1}; k_S = N/A.
Water film: O_3: $k_w = 4.8 \times 10^{-7}$ s^{-1}; $k_S = 1.5 \times 10^{-6}$ s^{-1}.
Water film: $O_2(^1\Delta_g)$: $k_w = 6.1 \times 10^{-6}$ s^{-1}; $k_S = 1.6 \times 10^{-4}$ s^{-1}.

There are a number of other cases in environmental chemistry where water surface acts as a heterogeneous catalyst [58]. Reactions in surface films of water on aerosols play a large role in the chloride chemistry of sea-salt aerosols [50]. It has been shown that the accumulation of polarizable anions (Cl^-) to the drop surface would enhance the surface phenomena. As a consequence, the surface reaction, $OH^{\bullet}(g) + Cl^-(ads) \rightarrow HOCl^{-\bullet}(aq)$ would lead to gaseous chlorine released to the atmosphere. Reaction of OH radicals with sea-salt particles to form sulfate in the troposphere has also been shown to be a heterogeneous surface reaction [51]. Vione et al [52] further confirmed that the surface reactions play a dominant role for photochemical reactions for very small droplets (~1 μm diameter). Reactions on surface ice films in polar stratospheric clouds play a major role in the destruction of the stratospheric ozone layer. Here, the reaction of Cl and ClO released from the UV photolysis of stable chlorofluorocarbons (CFCs) occur on surfaces of ice particles; this reaction derives mainly contributions from the heterogeneous reactions of CFCs adsorbed to ice. Once again, the kinetics of the heterogeneous reaction is such that the overall turnover rates are large and this alone helps explain the fast ozone disappearance rates [53,54]. Surface complexes of a number of gases such as SO_2 have also been invoked to explain theoretically and experimentally observed enhanced reaction rates at the water surface [55,56]. Water has also been to shown to act as a catalyst in radical-molecule atmospheric reactions [59]. Surface adsorption is also important in several other environmental interfaces such as air bubbles in water, water films in subsurface soil environments, and in environmental analytical chemistry applications [57].

ACKNOWLEDGMENTS

This research was supported by grants from the National Science Foundation (ATM 0082836 and ATM 0355291).

REFERENCES

1. L. J. Thibodeaux. *Environmental Chemodynamics*, John Wiley, New York (1997).
2. K. T. Valsaraj. *Elements of Environmental Engineering*, 2nd ed., CRC/Lewis Publishers, Boca Raton (2000).
3. A. Hartkopf, B. Karger. *Acc. Chem. Res*. **6**, 209 (1973).

4. C. Kemball, E. Rideal. *Proc. R. Soc. London* **A187**, 53 (1946).
5. M. Blank, R. Ottewill. *J. Phys. Chem.* **68**, 2206 (1964).
6. F. Hauxwell, R. Ottewill. *J. Colloid Interface Sci.* **28**, 514 (1968).
7. R. Ottewill, D. Jones. *Nature* **166**, 687 (1950).
8. R. Aveyard, D. Haydon. *Trans. Faraday. Soc*. **61**, 2255 (1965).
9. D. Baumer, G. H. Findenegg. *J. Colloid Interface Sci.* **85**, 118 (1982).
10. R. Massoudi, A. D. King. *J. Phys. Chem.* **78**, 2262 (1974).
11. R. Braunt, M. Conklin. *J. Phys. Chem. B* **104**, 11146 (2004).
12. D. Donaldson. *J. Phys. Chem. A* **103**, 62 (1999).
13. D. Donaldson, D. Anderson. *J. Phys. Chem. A* **103**, 871 (1999).
14. G. Dorris, D. Gray. *J. Phys. Chem.* **85**, 3628 (1981).
15. J. Hoff, D. Mackay, R. Gillham, W. Y. Shiu. *Environ. Sci. Technol*. **27**, 2174 (1993).
16. S. Raja, F. Yaccone, R. Ravikrishna, K. Valsaraj. *J. Chem. Eng. Data* **47**, 1213 (2002).
17. C. Roth, K.-U. Goss, R. Schwarzenbach. *J. Colloid Interface Sci*. **252**, 21 (2002).
18. J. Chen, K. Valsaraj. *J. Phys. Chem. A* **110**, 9161 (2006).
19. K.-U. Goss. *Environ. Sci. Technol*. **28**, 640 (1994).
20. M. Abraham. *J. Chromatogr.* **644**, 95 (1993).
21. M. Abraham, H. Chadha, G. Whiting, R. Mitchell. *J. Pharm. Sci*. **83**, 1085 (1994).
22. C. Kelly, C. Cramer, D. Truhlar. *J. Phys. Chem. B* **108**, 12882 (2004).
23. R. Vacha, P. Jungwirth, J. Chen, K. Valsaraj. *Phys. Chem. Chem. Phys*. **8**, 4461 (2006).
24. L. B. Partay, P. Jadlovszky, P. N. M. Hoang, S. Picaud, M. Mezei. *J. Phys. Chem. C* **111**, 9407 (2007).
25. L. Dang, D. Feller. *J. Phys. Chem. B* **104**, 4403 (2000).
26. J. Chen, F. Ehrenhauser, K. Valsaraj, M. Wornat. In *Atmospheric Aerosols: Characterization, Chemistry, Modeling, and Climate*, K. T. Valsaraj, R. R. Kommalapati (Eds.), ACS Symposium Series No. 1005, pp. 127–146, American Chemical Society, Washington, DC (2009).
27. E. S. Enami, M. R. Hoffmann, A. J. Colussi. *J. Phys. Chem. B* **112**, 4153 (2008).
28. D. E. Glotfelty, J. N. Seiber, A. Liljedahl. *Nature* **325**, 603 (1987).
29. D. J. Donaldson, B. T. Mmereki, S. R. Chaudhuri, S. Handley, M. Oh. *Faraday Discuss.* **130**, 227 (2005).
30. T. F. Kahan, D. J. Donaldson. *J. Phys. Chem. A* **111**, 1277 (2007).
31. K. T. Valsaraj, G. J. Thoma, D. D. Reible, L. J. Thibodeaux. *Atmos. Environ*. **27**, 203 (1993).
32. S. Raja, K. T. Valsaraj. *Atmos. Res.* **81**, 277 (2006).
33. R. G. Remorov, C. George. *Phys. Chem. Chem. Phys*. **8**, 4897 (2006).
34. P. Nissenson, C. J. H. Knox, B. J. Finlayson-Pitts, L. F. Phillips, D. G. Dabdub. *Phys. Chem. Chem. Phys*. **8**, 4700 (2006).
35. R. Vacha, P. Slavicek, M. Mucha, B. J. Finlayson-Pitts, P. Jungwirth. *J. Phys. Chem. A* **108**, 11573 (2004).
36. Y. Wadia, D. J. Tobias, R. Stafford, B. J. Finlayson-Pitts. *Langmuir* **16**, 9321 (2000).
37. T. F. Kahan, D. J. Donaldson. *Geophys. Res. Lett.* **10**, 1609 (2008).
38. S. Du, J. S. Francisco. *J. Phys. Chem. A* **112**, 4826 (2008).
39. S. Suzuki, P. G. Green, R. E. Baumgarner, S. Dasgupta, W. A. Goddard III, G. A. Blake. *Science* **257**, 942 (1992).
40. C. Vidal-Madjer, G. Guiochon, B. L. Karger. *J. Phys. Chem*. **80**, 394 (1976).
41. K. T. Valsaraj, D. J. Wilson. *Colloids Surf.* **8**, 203 (1983).
42. U. Poschl. *J. Aerosol Med. A* **15**, 203 (2002).
43. P. B. Petersen, R. J. Saykally. *Ann. Rev. Phys. Chem.* **57**, 333 (2006).
44. G. L. Richmond. *Ann. Rev. Phys. Chem*. **52**, 357 (2001).
45. K. B. Eisenthal. *Ann. Rev. Phys. Chem*. **43**, 627 (1992).
46. R. Mendelsohn, J. W. Brauner, A. Gericke. *Ann. Rev. Phys. Chem*. **46**, 305 (1995).

47. R. Vacha, L. Cwiklik, J. Rezac, P. Hobza, P. Jungwirth, K. Valsaraj, S. Bahr, V. Kempter. *J. Phys. Chem. A* **112**, 4942 (2008).
48. L. Partay, P. Jedlovsky, P. Hoang, S. Picaud, M. Mezei. *J. Phys. Chem. C* **111**, 9407 (2007).
49. D. E. Starr, E. K. Wong, D. R. Worsnop, K. R. Wilson, H. Bluhm. *Phys. Chem. Chem. Phys.* **10**, 3093 (2008).
50. E. M. Knipping, M. J. Lakin, K. L. Foster, P. Jungwirth, D. J. Tobias, R. B. Gerber, D. Dabdub, B. J. Finlayson-Pitts. *Science* **288**, 301 (2000).
51. A. Laskin, D. J. Gaspar, W. Wang, S. W. Hunt, J. P. Cowin, S. D. Colson, B. J. Finlayson-Pitts. *Science* **301**, 340 (2005).
52. D. Vione, C. Minero, A. Hamraoui, M. Privat. *Atmos. Environ*. **41**, 3303 (2007).
53. R. Bianco, J. T. Hynes. *Acc. Chem. Res.* **39**, 159 (2006).
54. S. Solomon. *Rev. Geophys*. **37**, 275 (1999).
55. J. H. Hu, Q. Shi, P. Davidovits, D. R. Wornsop, M. S. Zahniser, C. E. Kolb. *J. Phys. Chem.* **99**, 8768 (1995).
56. T. L. Tarbuck, G. L. Richmond. *J. Am. Chem. Soc*. **128**, 3256 (2006).
57. D. Mackay, W. Y. Shiu, K. T. Valsaraj, L. J. Thibodeaux. In *Air-Water Mass Transfer*, S. C. Wilhelms, J. S. Gulliver (Eds.), American Society of Civil Engineers, New York (1991).
58. A. L. Sumner, E. J. Menke, Y. Dubowski, J. T. Newberg, R. M. Penner, J. C. Hemminger, L. M. Wingen, T. Brauers, B. J. Finlayson-Pitts. *Phys. Chem. Chem. Phys.* **6**, 604 (2004).
59. E. V. Martinez, B. Hansmann, H. Hernandez, J. S. Francisco, J. Troe. B. Abel. *Science* **315**, 497 (2007).
60. E. Sato, K. Matsumoto, H. Okochi, M. Igawa. *Bull. Chem. Soc. Jpn*. **79**, 1231 (2006).
61. H. Okochi, M. Katinawa, D. Sugimoto, M. Igawa. *Atmos. Environ.* **39**, 6027 (2005).